Pulsed Nuclear Magnetic Resonance (NMR)
Spin-Lattice and Spin-Spin Relaxation Times in Applied Magnetic Fields

Keenan McConkey[1]
Faculty of Engineering Physics, University of British Columbia

(Dated: 9 March 2021)

The precession of nuclear magnetic moments in applied DC fields was investigated. In numerical simulation, magnetic moments were rotated using pulsed sequences of RF magnetic field, showing that spin-lattice relaxation time can be extracted from the transverse magnetic moment by varying pulse delay. Numerical simulation was also conducted for inhomogeneous DC fields; in this regime it was shown that the spin-spin relaxation time can be extracted by the observation of "spin-echo" phenomenon. Analysis was also performed on experimental data, demonstrating that numerical simulation predicted spin-lattice and spin-spin relaxation times determined from pulse sequence experiments.

I. INTRODUCTION

Nuclear Magnetic Resonance (NMR) is an effect which has well-studied in physics[1,2] and has been put to use in a number of fields, notably in medicine as MRI (Magnetic Resonance Imaging)[3], and in chemistry as a method for organic compound spectroscopy[4]. It has even been explored in the field of quantum computing as a method for ensemble computation[5].

The concept of spin in subatomic particles was already established in the 1920s, where experimental work made apparent that many features in atomic spectra could only be a result of nuclei possessing spin and magnetic moment. The effect in bulk materials was not reported until 1946 however by Bloch and Purcell, who would go on to win the Nobel Prize in Physics for their work[6]. The topic garnered significant interest from this point on; improvements in magnet homogeneity were made rapidly, eventually leading to the widespread use of NMR instruments in numerous fields of study.

The effect is quantum mechanical in nature: many nuclei, including the proton, produce a magnetic moment arising from their spin angular momentum. When placed in a direct current (DC) magnetic field, these magnetic moments tend to align with the applied field. One can then rotate the net magnetization to an arbitrary angle using a pulse of radio frequency (RF) magnetic field, from where the magnetization will decay back to equilibrium. Information about the nuclei's environment can then be determined based on differences between the decay of the transverse magnetization versus that of the component parallel to the magnetic field.

II. THEORY

A. Free Precession of a Proton

For preliminary numerical simulation, we consider the magnetic moment of single free proton, i.e. a single hydrogen nucleus. We ignore the quantum-mechanical behaviour of this proton and classically model it as a spinning charged sphere, meaning it has a magnetic moment $\vec{\mu}$ and angular momentum $\vec{J}$ related by:

$$\vec{\mu} = \gamma \vec{J} \tag{1}$$

Where γ is the proton's gyromagnetic ratio (approximately $2.675 \times 10^8 \mathrm{rad}/(\mathrm{s}\cdot\mathrm{T})$ for a proton). If we apply a DC magnetic field to this proton, the torque $\vec{\tau}$ it feels will be given by $\vec{\mu} \times \vec{B}$. Thus using (1) and relating torque to angular momentum via $\vec{\tau} = d\vec{J}/dt$, we can derive an ordinary differential equation (ODE) for the magnetic moment of a single proton:

$$\vec{\mu} \times \vec{B} = \frac{1}{\gamma} \frac{d\vec{\mu}}{dt} \tag{2}$$

For the a ensemble of protons with net magnetic moment $\vec{M}$, the same relationship holds. Going forward, we use $\vec{M}$ to refer to either the single proton or ensemble case for convenience.

$$\frac{d\vec{M}}{dt} = \gamma \vec{M} \times \vec{B} \tag{3}$$

We take DC field $\vec{B}$ to be entirely in the positive $\hat{z}$ direction, i.e. $\vec{B} = B_0 \cdot \hat{z}$ where $B_0 = 0.88T$ in the experimental setup. Clearly then (3) implies that the magnetic moment in the applied direction M_z will remain constant, while the transverse magnetic moment M_{xy} will precess with precessional frequency $\omega_0 = \gamma B_o$ (which can be derived as the resonant frequency of the spin state system using a magnetic energy based approach).

Results for numerical simulation of this precession are shown in FIG. 1. Units of Bohr magnetons are used to allow for magnetic strength values on the order of 10^0. Initial conditions are flexible since we cannot assume any initial spin orientation for the proton; we simply choose conditions that produce a phase difference between transverse components. By matching sinusoids, we confirm that both transverse components M_x and M_y precess at the resonance frequency ω_0.

B. Spin-Lattice and Spin-Spin Relaxation Time

We now simulate the net magnetization of a sample containing an ensemble of protons placed in a DC field. The sample's equilibrium magnetization doesn't just appear, rather M_z grows towards equilibrium when initially placed in the field, or when M_z is displaced from equilibrium. The growth of M_z towards equilibrium M_o is governed by a time constant T_1,

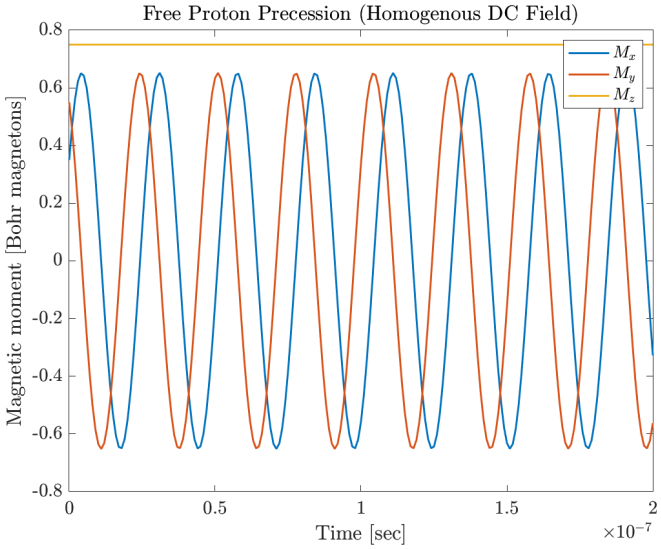

FIG. 1. Numerical simulation of a single proton's magnetic moment precession in a DC field at thermal equilibrium. Since the proton is free we can ignore spin-spin and spin-lattice interactions. As such, M_x and M_y precess at the resonant frequency ω_0 while M_z remains constant at equilibrium. We have flexibility in choosing the initial conditions of the proton's spin, since we cannot make any assumptions about its orientation. Here we choose conditions that produce an appropriate phase difference between M_x and M_y.

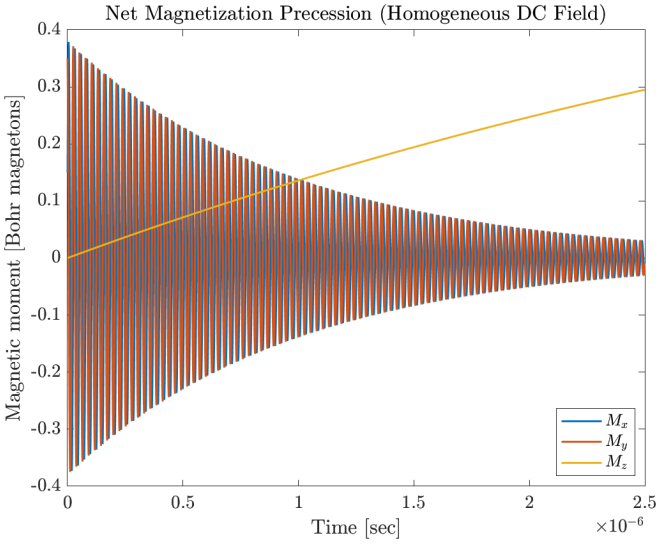

FIG. 2. Numerical simulation of net magnetic moment in a homogeneous DC field including spin-lattice and spin-spin relaxation times T_1 and T_2. The aligned magnetization M_z grows towards equilibrium while the transverse component M_{xy} precess in phase while decaying to zero. Simulation values of $T_1 \sim 5\mu$s, $T_2 \sim 1\mu$s, and $M_o = 1$ Bohr magnetons to produce typical precession behaviour: M_{xy} decays quickly because spin-spin interaction causes any in phase M_{xy} to rapidly dephase and cancel out, while M_z takes longer to reach equilibrium. Note the difference in time scale in relation to FIG. 1.

which we call spin-lattice relaxation time:

$$\frac{dM_z(t)}{dt} = \frac{M_o - M_z(t)}{T_1} \tag{4}$$

As was the case with the free proton, the individual proton's transverse spins will precess at frequency ω_0, but since the protons all start with random phases, the net transverse magnetization M_{xy} will sum to zero. However, if we make the magnetic moments rotate in phase in the xy plane, this combination of spin-up and spin-down states will decay exponentially with time constant T_2, which we call the spin-spin relaxation time:

$$\frac{dM_{xy}}{dt} = -\frac{M_{xy}(t)}{T_2} \tag{5}$$

This observed decay is a combination of the T_1 processes and the individual proton spins interacting with each other. Each individual spin is affected by both the applied DC field $\hat{B}$ and the field exerted by its neighbouring spins, which over time push the spin from in-phase to randomly-phased, resulting in a net transverse moment that decays to zero.

We can reduce equations (4) and (5) into a single ODE by introducing two new variables $\vec{M}_o$ and T_{inv}:

$$T_{\text{inv}} := \begin{bmatrix} T_2^{-1} & 0 & 0 \\ 0 & T_2^{-1} & 0 \\ 0 & 0 & T_1^{-1} \end{bmatrix}$$

$$\vec{M}_o := \begin{bmatrix} 0 & 0 & M_o \end{bmatrix}$$

Giving us a new ODE that accounts for both spin-spin and spin-lattice decay:

$$\frac{d\vec{M}(t)}{dt} = \gamma\vec{M} \times \vec{B} - T_{\text{inv}}\left(\vec{M} - \vec{M}_0\right) \tag{6}$$

Numerical simulation of ODE (6) is shown in FIG. 2. Simulation values of $T_1 = 5\ \mu$s and $T_2 = 1\ \mu$s were chosen to expected precession behaviour: M_{xy} will quickly dephase and decay because of spin-spin interaction, while M_z grows towards equilibrium at a slower rate.

C. π and $\frac{\pi}{2}$ Pulses

Using a RF magnetic field at ω, we can rotate the magnetization to an artibtrary angle determined by the length of the RF pulse. If we add our original DC field to this rotating (circularly polarized) RF field , our total field (working in the rotating coordinates of the RF field) is:

$$\vec{B}^*_{\text{eff}} = B_1\hat{x}^* + \left(B_o - \frac{\omega}{\gamma}\right)\hat{z}^* \tag{7}$$

Thus when the RF field frequency is tuned to resonance $\omega = \omega_0$, the second term disappears leaving us with a new magnetic moment ODE during the RF pulse:

$$\frac{d\vec{M}}{dt} = \gamma\vec{M} \times \vec{B}_{\text{eff}} = \gamma\vec{M} \times \vec{B}_1 \tag{8}$$

If we turn off B_1 as soon as $\vec{M}$ aligns with xy plane, we have a coherent magnetization entirely in the transverse directions. We call this a $\frac{\pi}{2}$ pulse. If we leave the pulse on for twice as long, $\vec{M}$ is flipped all the way around into $-\hat{z}$, which we call a π pulse.

As a consequence of our experimental setup, we cannot measure the magnetization that occurs along the same direction of $\vec{B}$, only the transverse components lying in the xy plane i.e. M_{xy}. Consequently, introduce a method for measuring T_1 using a $\pi \xrightarrow{\tau} \frac{\pi}{2}$ pulse sequence. Initially, the π pulse flips M_z into the negative direction, where it begins exponential growth back to equilibrium. After a delay of τ, the $\frac{\pi}{2}$ pulse rotates M_z into M_{xy}, where it precess briefly. We can then measure T_1 by fitting an exponential to the decay in max amplitude of M_{xy} for varying τ, i.e. the M_{xy} observed right after the $\frac{\pi}{2}$ pulse.

Numerical simulations of the $\pi \xrightarrow{\tau} \frac{\pi}{2}$ pulse sequence for two values of τ are shown in FIG. II C. ODE (8) is solved when RF pulse is on, otherwise ODE equation (6) is used. A π pulse length of 13.3 ns was determined to flip into M_z exactly into $-\hat{z}$. We confirm that we are able to recover T_1 by the method of varying τ. In this homogeneous field simulation, we can also recover T_2 from the decay of M_{xy} after the $\frac{\pi}{2}$ pulse using a mixer signal (explained further in the Experiment section). Experimentally, the T_2 we observe with this method will not be correct, which requires further explanation.

D. Introducing Inhomogeneity

One would think to measure T_2 from $\pi \xrightarrow{\tau} \frac{\pi}{2}$ pulse sequence by looking at the decay curve of M_{xy} after the $\frac{\pi}{2}$ pulse. This is called the Free Induction Decay (FID). Unfortunately, inhomogeneities in the magnet used to apply the DC field cause M_{xy} to decay faster than the T_2 of the sample for values of $T_2 > 0.3$ ms, which is common.

We introduce a field fluctuation to capture the variation in magnetic field felt by individual protons in the sample ensemble. The field felt by proton k is given by:

$$B_k = B_0 + \delta B_k \tag{9}$$

Where δB_k is a fluctuation sampled from a normal distribution of zero mean and variance σ. We treat σ as a parameter we can modify to model the inhomogeneity of the magnet.

Numerical simulation of an ensemble of $n = 500$ protons in an inhomogeneous DC field is shown in FIG. 4. T_1, T_2, and are left unmodified, and a value of $\tau = 0.3$ μs is used. The net magnetization is a result of sampling inhomogeneous field B_k from a normal distribution of $\sigma = 0.1$ for each proton and averaging the individual magnetic moments. T_2 is much lower than in the homogeneous field regime as expected. The reduction in T_2 was found to be proportional to the σ of the fluctuation function, i.e. the higher σ the further we are away from the homogeneous field regime. Run times were improved by forcing M_z into the rotations generated by the π and $\frac{\pi}{2}$ pulses rather than integrating ODE (8). Since the number of protons in our simulated ensemble is quite low, some sinusoidal noise occurs between pulse signals because some modes can still exist in the fluctuation function.

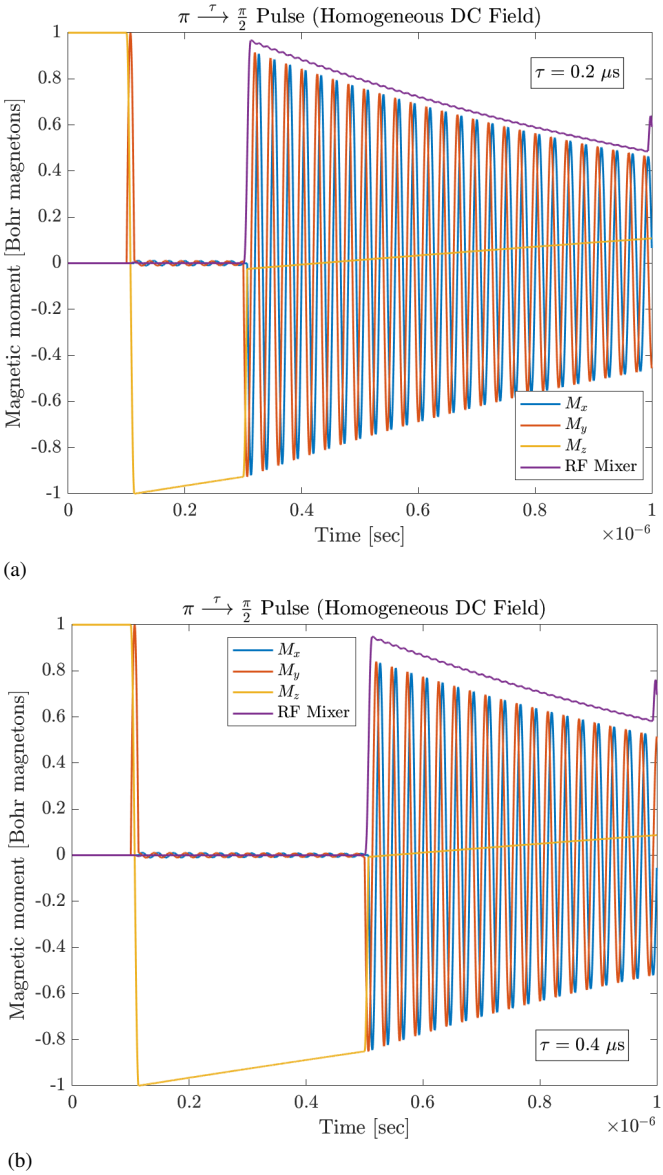

FIG. 3. Numerical simulation of the $\pi \xrightarrow{\tau} \frac{\pi}{2}$ pulse sequence in a homogeneous field. M_z is initially flipped into $-\hat{z}$, where it decays until it is flipped into M_{xy}, where it precesses and decays rapidly. We reuse time constants of $T_1 \sim 5$ μs and $T_2 \sim 1$ μs. Pulse delays of $\tau = 0.2$ μs, and $\tau = 0.4$ μs are shown in (a) and (b) respectively; we can recover T_1 from varying τ by fitting an exponential to the maximum amplitude of M_{xy} after the $\frac{\pi}{2}$ flip. We can also recover T_2 by looking at the decay of the mixer signal, which multiples M_x and the RF oscillator at frequency ω_0.

E. Modelling Spin Echo

We can now introduce a method for measuring T_2 with magnet inhomogeneity cancelled out by using a $\frac{\pi}{2} \xrightarrow{\tau} \pi$ pulse se-

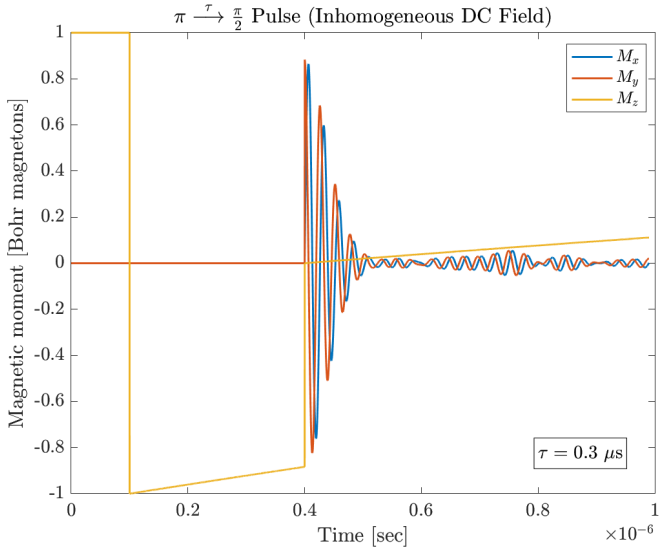

FIG. 4. Numerical simulation of the $\pi \xrightarrow{\tau} \frac{\pi}{2}$ pulse sequence in an inhomogeneous DC field. Simulation values of $T_1 \sim 5\ \mu$s and $T_2 \sim 1\ \mu$s and $\tau = 0.3\ \mu$s are used. As in the homogeneous case M_z is flipped into $-\hat{z}$, where it decays until it is flipped into M_{xy}, where it precesses and decays very rapidly. The observed T_2 however has been decreased significantly according to the variance of the introduced fluctuation in the field felt by each proton in the ensemble (here $\sigma = 0.1$), simulating real-world magnet inhomogeneity.

quence. We first rotate M_z into the xy plane using a $\frac{\pi}{2}$ pulse; after a time of τ we rotate the remaining M_{xy} with a π pulse. This second pulse causes the dephasing due to the magnet's inhomogeneity to be reversed, allowing the spins to rephase another τ time later, which we call a spin-echo. We can measure the true value T_2 by varying τ and observing the decay in the amplitude of the echo. Since the spin-echo occurs after a total delay of 2τ, the observed time constant will be twice that of the true T_2.

Numerical simulation of the spin-echo phenomena for two values of τ is shown in FIG. 5. Values of $T_1 = 5\ \mu$s, $T_2 = 1\ \mu$s, and $\sigma = 0.1$ are reused from previous simulations. The spin-echo occurs after a delay of 2τ as expected. Fitting an exponential to the max amplitude of the spin-echo for varying τ recovers a time constant of $\frac{T_2}{2}$. Again we forced M_z into the rotations expected from the π and $\frac{pi}{2}$ pulses rather than integrating ODE (8), and see some sinusoidal noise occur between pulses.

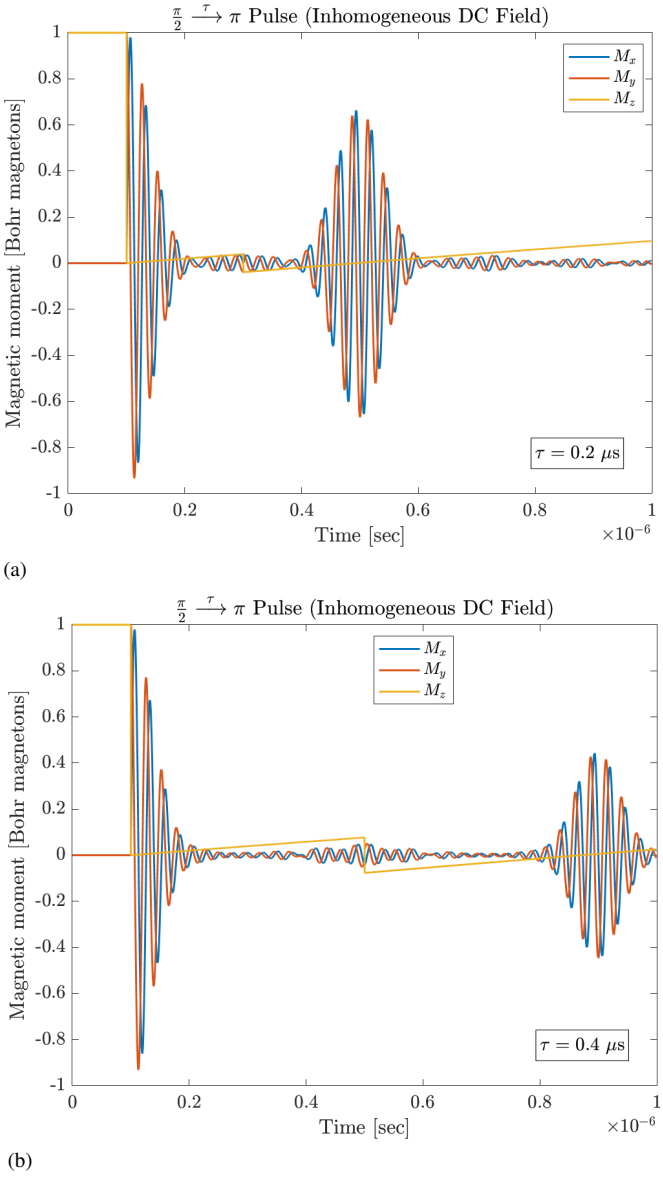

FIG. 5. Numerical simulation of the $\frac{\pi}{2} \xrightarrow{\tau} \pi$ pulse sequence in an inhomogeneous DC field. Simulated values of $T_1 = 5\ \mu$s, $T_2 = 1\ \mu$s, and $\sigma = 0.1$ have been left unchanged. Pulse delays of $\tau = 0.2\ \mu$s, and $\tau = 0.4\ \mu$s are shown in (a) and (b) respectively. A spin-echo is observed after a delay of 2τ due to spin rephasing. Fitting an exponential to the amplitude of the echo for varying τ retrieves a time constant of $T_2/2$, cancelling out the inhomogeneity of the magnet.

III. EXPERIMENT

A. Apparatus

A glass vial containing the sample to be magnetized is placed in inside a set of three mutually orthogonal coils, as pictured in FIG. 6. A water-cooled electromagnet provides the large DC field (0.88 T at 10A) applied to the sample. A smaller transmitter Hemholtz coil is located on either side of the magnet when viewing it directly. Finally, a third small coil is wrapped around the insertion point of the sample vial, where it acts as a receiver. As mentioned in Section II B, magnetization can only be measured in the direction transverse to the applied field (i.e. in the xy plane). This is because M_{xy} rotating at frequency ω_0 will induce an alternating current (AC) signal in the receiver coil, since the coil will be orthogonal to the axis of rotation of M_{xy}. Meanwhile M_z does not rotate and thus will not produce any AC signal.

The AC signal measured by the receiver coil is the basis for our NMR spectrometer, as shown in FIG. 7. Also contained

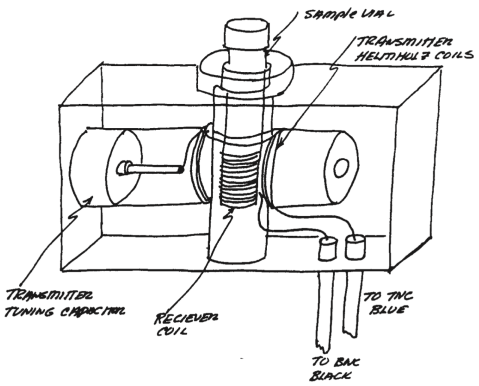

FIG. 6. A sketch of the probe system used to measure transverse magnetization of a sample. The sample is placed between three orthogonal coils: an electromagnet which creates the applied DC field, and two smaller Hemholtz coils, one of which is the receiver and the other the transmitter. Since M_{xy} rotates at angular frequency ω_0 as it precesses, it produces an AC signal in the receiver coil. Image Source: ENPH 352 Lab Manual[7].

within is a master oscillator, pulse programmer, and mixer. The master oscillator is used as the source for the RF magnetic field, while the pulse programmer turns RF on for short periods of time. The mixer is used to extract a decay curve from the AC receiver signal by multiplying it with master oscillator, which must be tuned to resonance to prevent beating.

FID waveform data for a sample of mineral oil was collected for both the $\pi \xrightarrow{\tau} \frac{\pi}{2}$ and $\frac{\pi}{2} \xrightarrow{\tau} \pi$ pulse sequences by tuning the pulse programmer settings appropriately. One must wait for at least $6T_1$ to $10T_1$ between pulse sequences to allow M_z to reach equilibrium. For mineral oil, this corresponds to a repetition time of about $100-200$ ms.

B. Sources of Noise and Uncertainty

A common source of noise in NMR is narrowband noise signals that operate at frequencies near the precession frequency of the protons, including power-line harmonics and other unknown sinusoidal sources of noise[8]. The AC receiver signal is also highly sensitive to fluctuations in the envirionment of the sample, with any slight variation in the applied DC field strength, RF field amplitude and phase, or receiver resonant frequency resulting in multiplicative noise in M_{xy}[9]. Both of the sources noises can be reduced by means of data anyalysis[8,9]. Their greatest impact is on the reproducibility of the experiment, which we aren't considering here.

From observation of the data collected, we can see significant noise in the observed FID signal. Since extracting T_1 and T_2 relies on determining the maximum value of the FID, this noise creates uncertainty in the true maximum of the signal.

IV. RESULTS

A. Extraction T_1 and T_2 from the $\pi \xrightarrow{\tau} \frac{\pi}{2}$ Pulse Sequence

A total of 40 $\pi \xrightarrow{\tau} \frac{\pi}{2}$ FID waveforms were collected for a mineral oil sample, with τ varying between 6 ms and 84 ms at intervals of 2 ms. The first four pulse sequences are shown in FIG. 8. We clearly see a decay pattern in the maximum amplitude of the FID, which can use to determine T_1.

We can formally determine T_1. The maximum amplitude of each of the 40 FID signals is determined and an exponential is fitted to the $V_{\max}$ vs τ curve using MATLAB's Curve Fitting Toolbox (which by default uses nonlinear least squares regression). When τ is less than the time it takes for M_z to grow back to zero after the π pulse, the $V_{\max}$ steadily decreases as τ increases. In the range where τ is larger than this zero time, the graph of max amplitude steadily increases as τ increases. We realize that we actually need to fit the difference between the max and the equilibrium value of M_z, i.e. $V_{\max} - V_o$ where V_o is the voltage at magnetization M_o. V_o was determined by matching time constants in the decaying and growing region. FIG. 9 shows the equilibrium corrected graph; from the exponential fit we recover:

$$T_1 = 39.25 \text{ ms} \tag{10}$$

We observe that the noise in the FID signal makes it difficult to determine its true maximum amplitude, so we assign it an uncertainty of ± 0.1 V, about half the fluctuation caused by noise (shown as the error bars in FIG. 9). MATLAB curve fitting gives us a 95% confidence interval (CI), which corresponds to a k factor of $k \approx 2$ ($k = 1.96$ in reality). Thus we can estimate uncertainty in T_1 for both the decay and growing regions from the CI bounds:

$$\sigma\left(T_{1,\text{ decay}}\right) = \frac{\frac{1}{23.94} - \frac{1}{27.09}}{2} = \pm 2.4 \text{ ms}$$

$$\sigma\left(T_{1,\text{ grow}}\right) = \frac{\frac{1}{24.41} - \frac{1}{26.47}}{2} = \pm 1.6 \text{ ms}$$

Averaging out we obtain:

$$\sigma(T_1) = \pm 2 \text{ ms} \tag{11}$$

We can also estimate T_2 by fitting to exponential to the FID decay waveform. An example of this fit is shown in FIG. 10. The time constant averaged out for three of these fits is only 520 ± 20 μs (uncertainty is due to acceptable range when curve fitting by eye), which is about two orders of magnitude lower than the T_2 we expect for mineral oil. Clearly, the magnet inhomogeneity has a significant effect on T_2 as was expected from simulation, so this not a good estimate of T_2.

B. Extraction of T_2 from the $\frac{\pi}{2} \xrightarrow{\tau} \pi$ Pulse Sequence

A total of 30 $\frac{\pi}{2} \xrightarrow{\tau} \pi$ spin echo waveforms were collected for a mineral oil sample, with τ varying between 5.5 ms and

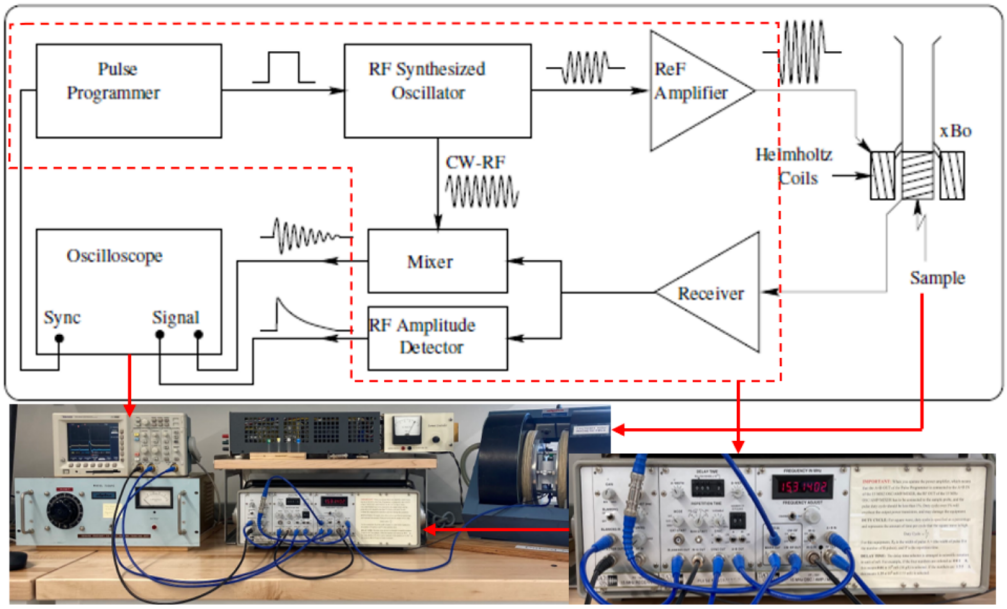

FIG. 7. Block diagram of the NMR spectrometer. A pulse programmer is paired with a master oscillator to generate pulsed sequences of RF field. The AC signal generated by the M_{xy} of the sample is mixed with the master oscillator signal to generate a FID waveform. This waveform and an amplitude detector for the AC signal are fed back into the oscilloscope for observation and data collection. Image Source: ENPH 352 Lab Manual[7].

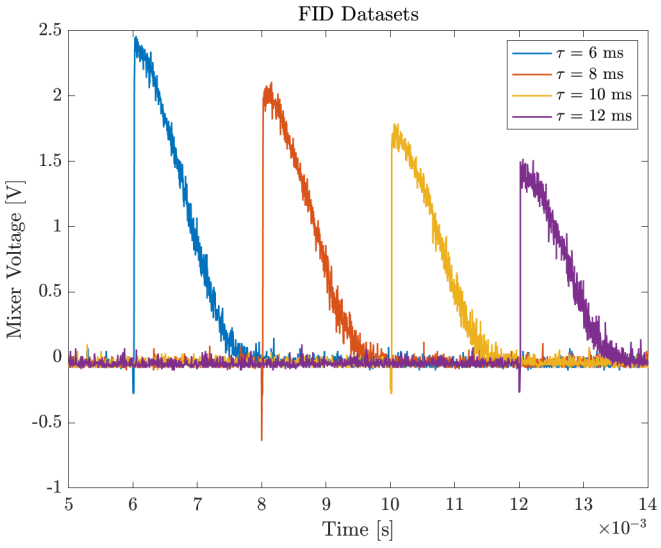

FIG. 8. FID waveforms for the $\pi \xrightarrow{\tau} \frac{\pi}{2}$ pulse sequence on mineral oil for the first four values of τ tested. Notice the clear decay pattern in the maximum amplitude of the FID signal, which we can use to determine T_1. We clearly see noise in the signals as which creates uncertainty in maximum amplitude.

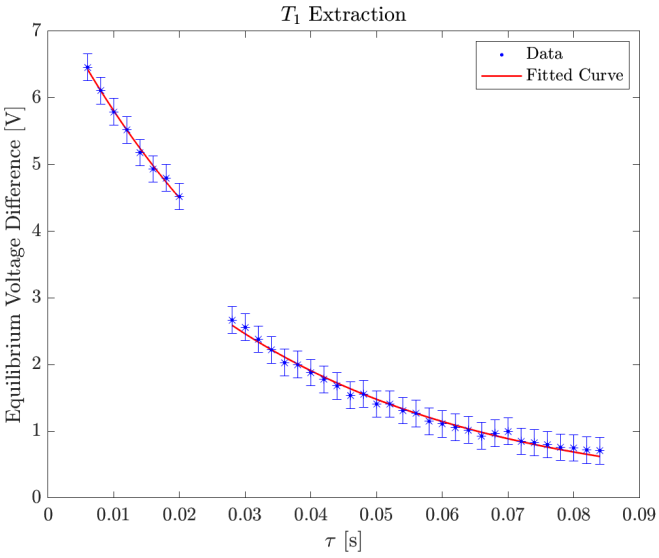

FIG. 9. Fitting en exponential to the equilibrium voltage difference $V_{\max} - V_o$ vs τ curve to extract a T_1 value of 39 ± 2 ms in mineral oil. $V_{\max}$ is the maximum voltage of the FID curve at each value of τ; the equilibrium voltage V_o was determined by matching time constants of the decaying and growing amplitude regions. Observe that the fit line passes through the error bounds resultant from the FID signal noise, so our fit is valid.

34.5 ms at intervals of 1 ms. FIG 11. shows the first four pulse sequences for τ from 5.5 ms to 8.5 ms. We clearly see a decay pattern in the maximum amplitude of the spin echo, which can use to determine T_2. We notice that the echo occurs after a delay 2τ as expected so we need to account for this when fitting an exponential.

We now formally determine T_2 by extracting the maximum amplitudes of the spin echo for each of the 30 waveforms and fitting an exponential to the $V_{\max,\text{echo}}$ vs 2τ graph using MATLAB's Curve Fitting Toolbox once again. Note that we fit

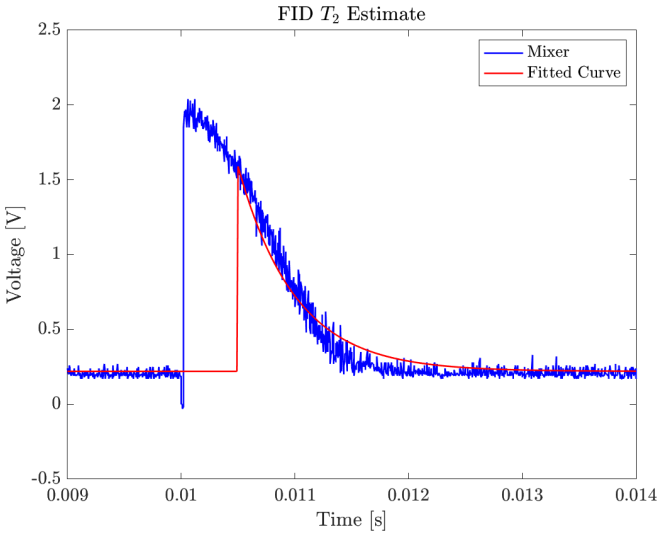

FIG. 10. Fitting an exponential to the FID decay to obtain a time constant estimate of 520 ± 20 μs without magnet inhomogeneity cancelled out. This is two orders of magnitude off the expected value of T_2 is mineral oil so magnet inhomogeneity is having a significant effect on T_2 as expected. Thus this is not a good estimate of T_2. Note that we fit an exponential to the tail end of the signal as it is fully exponential here.

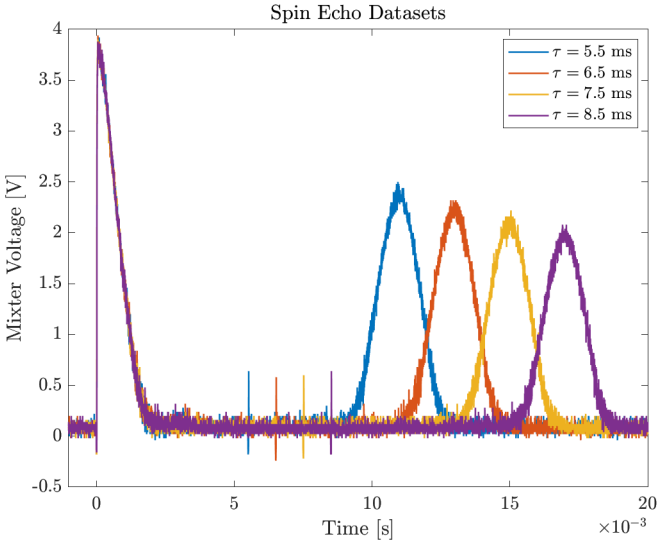

FIG. 11. Spin echo waveforms for the $\frac{\pi}{2} \xrightarrow{\tau} \pi$ pulse sequence on mineral oil for the first four values of τ tested. Notice the clear decay pattern in the maximum amplitude of the spin echo signal which occurs at 2τ, which we can use to determine T_2. Again the noise in the signals as creates uncertainty in maximum amplitude.

to 2τ to account for the doubled delay time of the spin echo. Since the spin echo goes to zero at high τ, we don't have to worry about fitting an equilibrium difference. FIG. 12 shows the exponential fit we obtain, from which we recover:

$$T_2 = 47.30 \text{ ms} \tag{12}$$

As was the case when determining T_1, the noise in the spin

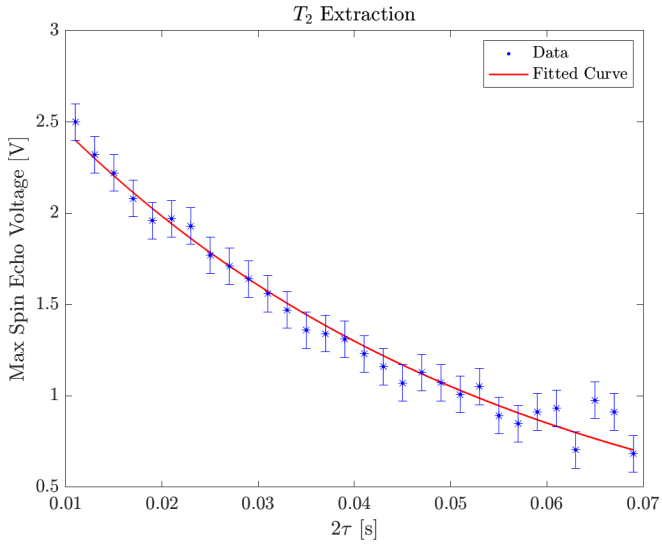

FIG. 12. Fitting an exponential to the maximum spin echo $V_{\text{max,echo}}$ vs. τ curve to extract $T_2 = 47 \pm 3$ ms in mineral oil with magnet inhomogeneity cancelled out. Note that we fit to 2τ as this is the delay at which the echo occurs. For high values of τ the curve does not fit within the error bars resultant from FID signal noise, it is possible that at low amplitudes the spin echo becomes difficult to detect.

echo signal makes it difficult to determine true maximum amplitudes, thus it has an uncertainty of ± 0.1 V (half the noise fluctuation), as shown in the error bars of FIG. 12. We again use the CI bounds to determine the uncertainty in T_2

$$\sigma(T_2) = \frac{\frac{1}{19.88} - \frac{1}{22.41}}{2} = 2.8 \text{ ms} \tag{13}$$

V. CONCLUSIONS

In summary, we confirmed the expected results of our numerical simulation in experimental data. As was predicted in simulation, by using the $\pi \xrightarrow{\tau} \frac{\pi}{2}$ pulse sequence to extract a maximal FID amplitude for varying delay times and fitting an exponential to this curve, we were able to determine the spin-lattice relaxation time of mineral oil:

$$T_1 = 39 \pm 2 \text{ ms}$$

An important note in determining T_1 was that we had to fit the equilibrium difference in the extracted maximum FID amplitude to account for the FID signal always being positive.

We also confirmed in both simulation and experimental data that magnet inhomogeneity causes the FID time constant to decrease significantly, and that the more inhomogeneous the magnet the greater the decrease in the time constant. We also showed that observing a spin echo created by $\frac{\pi}{2} \xrightarrow{\tau} \pi$ pulse sequence allows us to extract the true value of the spin-spin relaxation time with magnet inhomogeneity cancelled out. By fitting an exponential to the spin echo amplitude vs. doubled

pulse delay curve we determined the spin-spin relaxation time in mineral oil:

$$T_2 = 47 \pm 3 \text{ ms}$$

It was important to account for the spin echo occurring at double the input pulse delay when determining the time constant.

We also determined the time constant of the FID curve to be 520 ± 20 μs. This result includes both the magnet inhomogeneity and the T_2 processes, so we can use it to determine factor of reduction caused by magnet inhomogeneity:

$$\text{Reduction Factor} = \frac{\text{FID Time Constant}}{T_2} = \frac{1}{214}$$

If desired, one could use this reduction factor and the results of our simulation in Section II D to match a variance in fluctuation distribution to the observed reduction in T_2, deducing a variance value for the inhomogeneity of the magnet.

Our observed uncertainties were reasonable, with error bars determined by receiver signal noise overlapping with the curve fitting of time constant values, except for some outliers in low amplitude signals. We expect noise in our experiment to occur (see Section III B) especially when extracting maximum amplitudes. We could try reducing this noise by filtering our receiver signal (e.g. 6th Order Butterworth) or by manually fitting a maximum amplitude to each τ value.

We could attempt to improve our results by implementing methods of noise reduction described in[8,9]. Numerical simulation could be improved by increasing the number of protons in our ensemble in order to minimize sinusoidal noise occurrence. More elaborate pulse sequences, such as the Carr-Purcell-Meiboom-Gill sequence[10], could also be explored as a method for improving results.

[1] A. Carrington and A. McLachlan, *Introduction to Magnetic Resonance with Applications to Chemistry and Chemical Physics* (Harper & Row, 1967).

[2] J. Hornak, *The Basics of NMR*, RIT Magnetic Resonance Laboratory, Center for Imaging Science, Rochester Institute of Technology, Rochester, NY 14623-5604 (1999).

[3] M. Idrees, "An overview on mri physics and its clinical applications," International Journal of Current Pharmaceutical and Clinical Research **4**, 185–193 (2014).

[4] J. Chou and R. Sounier, "Solution nuclear magnetic resonance spectroscopy," Methods in molecular biology (Clifton, N.J.) **955**, 495–517 (2013).

[5] N. A. Gershenfeld and I. L. Chuang, "Bulk spin-resonance quantum computation," Science **275**, 350–356 (1997), https://science.sciencemag.org/content/275/5298/350.full.pdf.

[6] E. D. Becker, "A brief history of nuclear magnetic resonance," Analytical Chemistry **65**, 295A–302A (1993).

[7] V. M. et al., *ENPH 352: Laboratory Techniques in Physics The Online Edition*, Department of Physics and Astronomy, University of British Columbia, 6224 Agricultural Road, Vancouver, British Columbia (2021).

[8] D. Grombacher, L. Liu, G. K. Osterman, and J. J. Larsen, "Mitigating narrowband noise sources close to the larmor frequency in surface nmr," IEEE Geoscience and Remote Sensing Letters , 1–5 (2020).

[9] J. Granwehr, "Multiplicative or t 1 noise in NMR spectroscopy," Applied Magnetic Resonance **32**, 113–156 (2007).

[10] L. P. McIntosh, "Cpmg," in *Encyclopedia of Biophysics*, edited by G. C. K. Roberts (Springer Berlin Heidelberg, Berlin, Heidelberg, 2013) pp. 386–386.